



Contents lists available at SciVerse ScienceDirect

Icarus

journal homepage: www.elsevier.com/locate/icarus

Note

Trapped Ar isotopes in meteorite ALH 84001 indicate Mars did not have a thick ancient atmosphere

William S. Cassata^{a,b,*}, David L. Shuster^{b,a}, Paul R. Renne^{b,a}, Benjamin P. Weiss^c^a Department of Earth and Planetary Science, University of California – Berkeley, 307 McCone Hall #4767, Berkeley, CA 94720-4767, USA^b Berkeley Geochronology Center, 2455 Ridge Road, Berkeley, CA 94709, USA^c Department of Earth, Atmospheric, and Planetary Sciences, Massachusetts Institute of Technology, 77 Massachusetts Avenue, Cambridge, MA 02139, USA

ARTICLE INFO

Article history:

Received 8 March 2012

Revised 30 April 2012

Accepted 4 May 2012

Available online 12 May 2012

Keywords:

Mars, Atmosphere

Mars, Climate

Atmospheres, Evolution

Cosmochemistry

ABSTRACT

Water is not currently stable in liquid form on the martian surface due to the present mean atmospheric pressure of ~ 7 mbar and mean global temperature of ~ 220 K. However, geomorphic features and hydrated mineral assemblages suggest that Mars' climate was once warmer and liquid water flowed on the surface. These observations may indicate a substantially more massive atmosphere in the past, but there have been few observational constraints on paleoatmospheric pressures. Here we show how the $^{40}\text{Ar}/^{36}\text{Ar}$ ratios of trapped gases within martian meteorite ALH 84001 constrain paleoatmospheric pressure on Mars during the Noachian era [~ 4.56 – 3.8 billion years (Ga)]. Our model indicates that atmospheric pressures did not exceed ~ 1.5 bar during the first 400 million years (Ma) of the Noachian era, and were < 400 mbar by 4.16 Ga. Such pressures of CO_2 are only sufficient to stabilize liquid water on Mars' surface at low latitudes during seasonally warm periods. Other greenhouse gases like SO_2 and water vapor may have played an important role in intermittently stabilizing liquid water at higher latitudes following major volcanic eruptions or impact events.

© 2012 Elsevier Inc. All rights reserved.

1. Introduction

The composition and mass of the ancient martian atmosphere are key parameters of planetary evolution that remain poorly understood. Radiative transfer models suggest that a greater pressures of greenhouse gases in the past (e.g., > 5 bars of CO_2) were necessary to sustain surface temperatures above freezing for prolonged durations (Jakosky and Phillips, 2001; Pepin, 1994; Colaprete and Toon, 2003; Pollack et al., 1987; Yung et al., 1997). Alternatively, large impacts may have vaporized subsurface volatiles and generated relatively brief periods of warm and wet conditions (e.g., 10^2 – 10^3 years; Segura et al., 2002), which may explain why a decrease in fluvial erosion appears to coincide with the end of the heavy impact bombardment (Catling and Leovy, 2007). Both explanations imply climate conditions during the Noachian era that were significantly different from the present. However, whereas prolonged periods of high concentrations of greenhouse gases implicate warm and wet surface environments conducive to life, intermittent impact-driven greenhouse events do not.

Observational constraints on past climate conditions on Mars are limited. The scarcity of carbonate minerals (Bandfield, 2002; Bibring et al., 2006; Murchie et al., 2009) (expected to form in low- SO_2 aqueous environments) and the apparently low partial pressures of CO_2 required to explain the alteration of Noachian surface rocks to clay minerals (0.001–0.01 bar; Chevrier et al., 2007) suggest that a dense CO_2 -rich atmosphere did not persist throughout the Noachian. The identification of sulfate deposits in the martian regolith (Arvidson et al., 2005; Gendrin et al., 2005; Squyres et al., 2004) indicates that atmospheric SO_2 and H_2S may have contributed to greenhouse warming. Modest influxes of SO_2 and H_2S (e.g., $\sim 2 \times 10^{-6}$ bar) in the presence of only 50 mbar CO_2 can promote transient periods of warm, wet conditions (Halevy et al., 2007; Johnson et al., 2008). Despite these

observations, whether a dense, CO_2 -rich atmosphere ever existed and the extent to which other greenhouse gases contributed to warming remain poorly understood.

Martian meteorites contain trapped atmospheric gases (Bogard et al., 2001) that provide chemical constraints on past atmospheric conditions. Cassata et al. (2010) identified a trapped argon (Ar) component within maskelynite in the 4.16 ± 0.04 Ga old martian meteorite ALH 84001 with an $^{40}\text{Ar}/^{36}\text{Ar}$ ratio of 626 ± 100 (Fig. 1). Here we present the first attempt to use this isotopic composition to constrain atmospheric pressure on Mars between the time of planetary formation and the 4.16 Ga age of the maskelynite. We discuss the implications of these pressure limits for greenhouse warming, atmospheric evolution, and climate on Mars during the Noachian era. Critical to our arguments is the assumption that the trapped argon component identified within maskelynite is atmospheric in origin and was emplaced in the meteorite at 4.16 Ga. The concordance of the maskelynite $^{40}\text{Ar}/^{36}\text{Ar}$ vs. $^{39}\text{Ar}/^{36}\text{Ar}$ isochron diagram (Fig. 1) provides strong support for such an interpretation; terrestrial feldspars and glasses with appreciably non-atmospheric trapped components generally fail to produce linear isochron diagrams (discussed in detail in the Supplementary Files).

2. An atmospheric ^{40}Ar evolution model

A comparison of the atmospheric $^{40}\text{Ar}/^{36}\text{Ar}$ ratios of Earth and Mars reveals significant differences in the evolution of the two atmospheres (Fig. 1). On Earth, the net transport of volatiles from the asthenosphere and lithosphere to the atmosphere has elevated the atmospheric $^{40}\text{Ar}/^{36}\text{Ar}$ ratio from its primordial ratio of $\sim 10^{-3}$ at 4.56 Ga (Begemann et al., 1976) to the present value of > 298 (Lee et al., 2006). Meteorite measurements indicate that on Mars, the atmospheric $^{40}\text{Ar}/^{36}\text{Ar}$ ratio increased from $\sim 10^{-3}$ at 4.56 Ga, to 626 ± 100 at 4.16 Ga, to the present value of ~ 1800 (Bogard et al., 2001). Thus, the net effects of martian planetary degassing and late stage planetary accretion increased the martian atmospheric $^{40}\text{Ar}/^{36}\text{Ar}$ ratio to more than twice the modern ratio on Earth, but over only $\sim 1/10$ the duration (~ 400 Ma). The relatively rapid evolution in the martian atmospheric $^{40}\text{Ar}/^{36}\text{Ar}$ ratio suggests that one or more of the following is true:

* Corresponding author at: Department of Earth and Planetary Science, University of California – Berkeley, 307 McCone Hall #4767, Berkeley, CA 94720-4767, USA.

E-mail addresses: cassata@berkeley.edu (W.S. Cassata), dshuster@bgc.org (D.L. Shuster), preenne@bgc.org (P.R. Renne), bpweiss@mit.edu (B.P. Weiss).

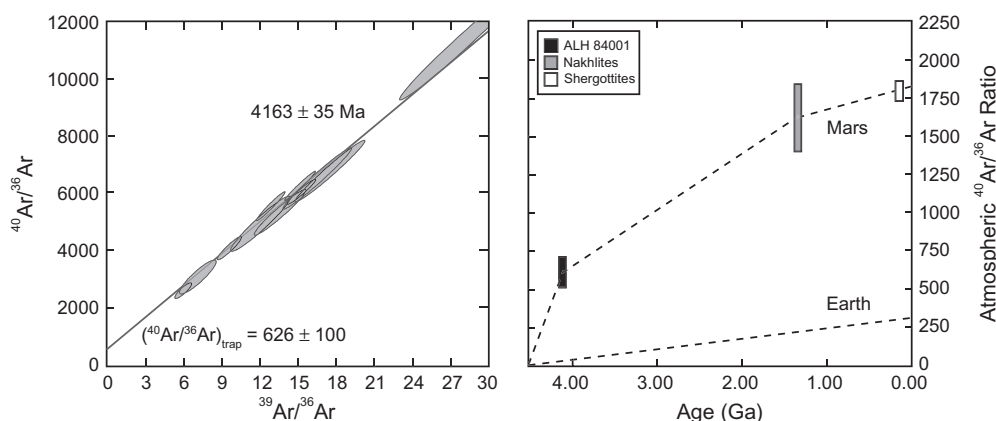


Fig. 1. Left: $^{40}\text{Ar}/^{39}\text{Ar}$ isochron diagram for maskelynite in ALH 84001-1 [redrafted from Cassata et al. (2010)]. Correlation between the isotope ratios $^{39}\text{Ar}/^{36}\text{Ar}$ and $^{40}\text{Ar}/^{36}\text{Ar}$ measured during stepwise degassing of ALH 84001 constrains the non-radiogenic argon component “trapped” in the glass from the y-intercept and the age from the slope. The isochron age (4.165 ± 0.035 Ga) is indistinguishable at 2σ from recently reported Lu–Hf (4.09 ± 0.03 Ga; Lapen et al., 2010) and Pb–Pb (4.074 ± 0.099 Ga; Bouvier et al., 2009) ages. The $^{40}\text{Ar}/^{36}\text{Ar}$ ratio of the trapped component in ALH 84001 maskelynite is 626 ± 100 . Right: Plot of the $^{40}\text{Ar}/^{36}\text{Ar}$ ratios of trapped Ar components identified in martian meteorites. ALH 84001 and Nakhilite data are from Cassata et al. (2010). Shergottite data are from Bogard et al. (2001). The Nakhilite $^{40}\text{Ar}/^{36}\text{Ar}$ ratio represents the weighted average of MIL 03346 and Nakhla meteorites (see Supplementary Files). Earth’s atmospheric $^{40}\text{Ar}/^{36}\text{Ar}$ ratio is shown for comparison. Dashed lines linearly connect data points and do not represent the evolution of the atmospheric $^{40}\text{Ar}/^{36}\text{Ar}$ ratio on Earth or Mars. We have used a young age for Shergottites. However, if the melt veins containing trapped atmospheric gases in EETA 79001 are older (e.g., >4 Ga), as suggested for the age of Shergottites by Bouvier et al. (2009), then the martian atmospheric $^{40}\text{Ar}/^{36}\text{Ar}$ ratio must have increased even faster than shown in this figure.

- (1) the potassium (K) concentration of Mars is greater than Earth, such that significantly more radiogenic ^{40}Ar was generated early on Mars,
- (2) the ^{36}Ar concentration of Mars’ interior is lower than Earth’s, such that extracted magmas had elevated $^{40}\text{Ar}/^{36}\text{Ar}$ ratios relative to terrestrial magmas of equivalent age and K concentration,
- (3) planetary degassing was more efficient on early Mars than Earth, such that a greater proportion of radiogenic ^{40}Ar was delivered from the astheno-lithosphere to the atmosphere, and/or
- (4) Mars had a thinner atmosphere than Earth (i.e., less atmospheric ^{36}Ar), such that a given quantity of degassed ^{40}Ar more efficiently elevated the atmospheric $^{40}\text{Ar}/^{36}\text{Ar}$ ratio.

In this paper, we use published constraints on (1)–(3) to assess whether or not (4) is a viable explanation for Mars’ elevated $^{40}\text{Ar}/^{36}\text{Ar}$ ratio at 4.16 Ga. We simulate planetary degassing under a broad range of atmospheric pressure conditions and explore the resulting evolution in the martian atmospheric $^{40}\text{Ar}/^{36}\text{Ar}$ ratio during the Noachian. Our objective is to place bounds on atmospheric pressures during the first ~400 Ma of martian history that are consistent with an $^{40}\text{Ar}/^{36}\text{Ar}$ ratio of 626 ± 100 at 4.16 Ga. We begin with the following postulates:

- (1) Mars was assembled from bodies that had an initial inventory of volatiles with $^{40}\text{Ar}/^{36}\text{Ar} < 10^{-3}$ (Begemann et al., 1976).
- (2) Planetary degassing and meteorite accretion added both radiogenic volatiles (^{40}Ar) and non-radiogenic volatiles (^{36}Ar , N_2 , and CO_2) to the atmosphere.
- (3) Atmospheric loss due to impact erosion removed volatiles, but did not fractionate ^{36}Ar and ^{40}Ar (Brain and Jakosky, 1998; Melosh and Vickery, 1989).
- (4) At 4.16 ± 0.04 Ga the atmospheric $^{40}\text{Ar}/^{36}\text{Ar}$ ratio was 626 ± 100 , as indicated by the trapped component in ALH 84001 maskelynite (Cassata et al., 2010).

Under these conditions, the atmospheric molar abundance of Ar isotope X varies through time according to the following equation:

$$\frac{d^X\text{Ar}}{dt} = N_X(t) - \left(X_{\text{Ar}} \frac{L(t)}{P(t)} \right), \quad (1)$$

where X_{Ar} denotes the total atmospheric abundance, $N_X(t)$ is the rate of addition of isotope X to the atmosphere due to planetary degassing and meteorite accretion, $P(t)$ is atmospheric pressure, and $L(t)$ is the rate of atmospheric pressure loss due to impact erosion. The latter are related by:

$$\frac{dP}{dt} = I(t) - L(t), \quad (2)$$

where $I(t)$ is the total rate of atmospheric pressure increase due to planetary degassing of all gaseous species, which is essentially equal to the rate of increase in CO_2 since it comprises >95% of the present atmosphere.

To constrain the initial martian atmospheric pressure and its subsequent evolution, we simulated a range of hypothetical paleoatmospheric pressure paths. In each scenario, $P(t)$ declines over time due to impact erosion of atmospheric gases (i.e., L remains greater than I). We assume that other escape processes that enrich ^{40}Ar

relative to ^{36}Ar (i.e., pick-up ion sputtering and hydrodynamic escape) were not significant during the first 400 million years of the Noachian due to the existence of a magnetic dynamo (Cassata et al., 2010; Brain and Jakosky, 1998; Hutchins et al., 1997; Roberts et al., 2009; Weiss et al., 2008). Only minor differences in the inferred atmospheric pressures would result if such processes were included in our model (discussed below). We allow for initial atmospheric pressures between 0.1 and 10 bar, and then explore various scenarios in which pressure declines either randomly, exponentially with the same scale parameter as that of the martian impact flux (Melosh and Vickery, 1989) (to approximate impact erosion in absence of planetary degassing), or linearly to final pressures of 0.01–1 bar at 4.16 Ga (to approximate an exponential rate of loss due to impact erosion damped by increases in pressure due to planetary degassing). Using these $P(t)$ curves and a planetary degassing model (discussed below), we then solved Eqs. (1) and (2) to constrain paleoatmospheric pressure paths that yield $^{40}\text{Ar}/^{36}\text{Ar}$ ratios of 626 ± 100 at 4.16 Ga. A detailed description of our implementation of Eqs. (1) and (2) is given in the Supplementary Files.

3. Model parameters

To calculate the production of atmospheric volatiles associated with surface, crustal, and upper mantle magmatic activity, we adopted the crustal growth model of Breuer and Spohn (2006) for an initial mantle temperature of 2000 K and no primordial crust (a summary of all model parameters is given in Table 1). Relative to other models, Breuer and Spohn (2006) predict a higher rate of magma production and, therefore, ^{40}Ar delivery to the atmosphere. Because a higher ^{40}Ar production rate demands higher atmospheric pressure (i.e., more atmospheric ^{36}Ar) to maintain a given $^{40}\text{Ar}/^{36}\text{Ar}$ ratio, using Breuer and Spohn (2006) places an upper bound on permissible atmospheric pressures during the Noachian. Less voluminous magmatic production models would predict up to an order of magnitude lower pressures during the Noachian. We assumed that magmas contain between 1300 ppm K (e.g., Nakhla meteorite; Dreibus et al., 1982) and 3300 ppm K (e.g., Mars’ crust; Taylor et al., 2006). To estimate the concentration of CO_2 in magmas we used values published for melt inclusions in martian meteorites, which typically range from 5 to 500 ppm (Boctor et al., 2005). This is consistent with estimates of magmatic CO_2 concentrations based on thermodynamic equilibrium between dissolved carbon and graphite in the martian mantle (50–500 ppm; Hirschmann and Withers, 2008), and measurements of CO_2 concentrations in MORB source regions (<250 ppm; Saal et al., 2002). No direct measurements of ^{36}Ar concentrations in martian meteorite melt inclusions have been published. We assumed that the $^{36}\text{Ar}/\text{CO}_2$ ratio observed in ALH 84001 pyroxenes ($\sim 10^{-8}$ – 10^{-9} ; Cassata et al., 2010; Boctor et al., 2006), reflects that of mantle melts.¹ The model results differ by less than approximately a factor of two over the ranges in assumed magmatic K, ^{36}Ar , and CO_2 concentrations (see Supplementary Files).

To model the mass of ^{40}Ar added to the atmosphere by asteroids, we used the martian impact flux derived by Melosh and Vickery (1989) from the lunar cratering record of Neukum and Wise (1976) following Manning et al. (2006) (see Supplementary Files). We assumed that impacting asteroids contain a chondritic abun-

¹ $^{36}\text{Ar}/\text{CO}_2$ ratio for ALH 84001 orthopyroxene based on 14–167 ppm CO_2 (Boctor et al., 2006) and 0.3 ppt ^{36}Ar (excludes cosmogenic ^{36}Ar ; Cassata et al., 2010).

Table 1

Definitions of model parameters and their values.

Parameter	Notation	Parameter range ^a	Preferred value	Unit	Ref.
Radius of Mars	r		3400×10^3	m	1
Mass of bulk silicate Mars (BSM) ^b	m_{BSM}		5.11×10^{23}	kg	2
Surface gravity	g		1700×10^3	m/s ²	1
K concentration in magmas	$[K]_{\text{magma}}$	1300–3300	2500	ppm	3, 4
K concentration in impactors	$[K]_{\text{impact}}$		550	ppm	5
³⁶ Ar concentration in impactors	$[^{36}\text{Ar}]_{\text{impact}}$		15	ppt	6
(N ₂ + CO ₂) concentration in magmas	$[CN]_{\text{magma}}$	5–500	250	ppm	7, 8, 9
Magmatic ³⁶ Ar/(N ₂ + CO ₂) ratio	R_{magma}	10^{-8} – 10^{-9}	5×10^{-9}		10, 11
Initial atmospheric ³⁶ Ar/(N ₂ + CO ₂) ratio	R_{atm}	10^{-4} – 10^{-6}	10^{-5}		
Magma flux ^c	$V_{\text{magma}}(t)$		Breuer and Spohn (2006)	kg/Ma	12
Magma density	ρ_{magma}		3000	kg/km ³	
Impactor flux ^d	$V_{\text{impact}}(t)$		Melosh and Vickery (1989)	kg/Ma	13, 14

1: Sohl and Spohn (1997); 2: Lodders and Fegley (1997); 3: Dreibus et al. (1982); 4: Taylor et al. (2006); 5: McDonough and Sun (1995); 6: Zahnring (1966); 7: Saal et al. (2002); 8: Boctor et al. (2005); 9: Hirschmann and Withers (2008); 10: Cassata et al. (2010); 11: Boctor et al. (2006); 12: Breuer and Spohn (2006); 13: Melosh and Vickery (1989); 14: Neukum and Wise (1976).

^a See text for details and Supplementary Files for an analysis of the model sensitivity to the parameter range.

^b Calculated assuming the martian core is 20 wt.% and BSM is 80 wt.%.

^c Breuer and Spohn (2006) is the crustal production model of Breuer and Spohn (2006) (see text for details).

^d Melosh and Vickery (1989) is the martian impact flux derived by Melosh and Vickery (1989) (see text for details).

dance of K (550 ppm; McDonough and Sun, 1995) and ³⁶Ar concentrations typical of H-, L-, and LL-chondrites (~15 ppt; Zahnring, 1966). Impact-derived ⁴⁰Ar is negligible in comparison to mantle-derived ⁴⁰Ar (<1%). We neglect the insignificant amounts of CO₂ and N₂ brought to Mars by impactors.

3.1. The initial atmospheric ³⁶Ar/(N₂+CO₂) ratio

The extent to which the addition of ⁴⁰Ar increases the atmospheric ⁴⁰Ar/³⁶Ar ratio is inversely proportional to the abundance of atmospheric ³⁶Ar. Thus, an important variable in our model is the primordial abundance of atmospheric ³⁶Ar, which, in an atmosphere composed primarily of N₂ and CO₂ can be expressed as initial atmospheric pressure (P_0) multiplied by the initial atmospheric ³⁶Ar/(N₂ + CO₂) ratio. The current martian atmospheric ³⁶Ar/(CO₂ + N₂) ratio is $\sim 10^{-5}$ (Bogard et al., 2001; Owen et al., 1977)², but this ratio may have been different in the past as atmospheric escape processes, mantle degassing, and authigenic mineralization of carbonates have fractionated N₂, CO₂, and Ar over time. To determine maximum atmospheric pressures during the Noachian we must estimate the minimum primordial ³⁶Ar/(CO₂ + N₂) ratio; the lowest value *a priori* implies the greatest abundance of atmospheric CO₂ and N₂ for a given quantity of ³⁶Ar. We will ultimately assume an initial atmospheric ³⁶Ar/(CO₂ + N₂) ratio of 10^{-5} for reasons discussed below.

Authigenic mineralization of carbonates enriches the relative concentration of atmospheric Ar by depleting CO₂. While spectral observations have not identified massive near-surface carbonate deposits (Bandfield, 2002; Bibring et al., 2006), carbonate has been discovered in outcrops in the Nili Fossae region (Michalski and Niles, 2010) and the Columbia Hills of Gusev crater (Morris et al., 2010; Christensen et al., 2004), in regolith at the Phoenix landing site (Boynton et al., 2009), and in some martian meteorites (e.g., ALH 84001). We can estimate the extent to which CO₂ has been depleted relative to other atmospheric gases by comparing Mars' volatile budget with that of other terrestrial planets (Owen and Bar-Nun, 1995). The atmospheres of Venus and Earth have similar C/N ratios of ~15 (Donahue and Polack, 1983) and 20 ± 10 (Owen and Bar-Nun, 1995), respectively, when CO₂ bound in carbonates is considered in the terrestrial inventory. The similarity of these planetary volatile ratios presumably reflects derivation from common meteoritic sources that were also parental to the martian atmosphere (Anders and Owen, 1977). Mars' atmospheric C/N ratio is not directly comparable to that of Earth and Venus because non-thermal escape processes have fractionated C and N over time. Based on Mars' heavy ¹⁵N/¹⁴N ratio (Jakosky and Phillips, 2001), these processes are estimated to have removed approximately 90% of Mars' atmospheric N not lost to space via impact erosion (Jakosky and Phillips, 2001). Assuming no loss of atmospheric CO₂ (as a limiting constraint to place an upper bound on CO₂ that might be contained in carbonates), the fractionation-corrected martian atmospheric C/N ratio is ~2. If we assume that the difference between this ratio and that of Earth and Venus (~15) reflects CO₂ bound in carbonates, then CO₂ has been depleted by up to ~87% (i.e., 13/15) relative to N. Similarly, Owen and Bar-Nun (1995) estimated that CO₂ has been depleted by 90% relative to Kr based on differences between the martian atmospheric ⁸⁴Kr/C ratio and that of Earth and Venus. The mass of near-surface carbonates associated with this CO₂ depletion depends on atmospheric pressures at times when deposition occurred.

The effect of the abovementioned CO₂ sequestration on the atmospheric ³⁶Ar/(CO₂ + N₂) would be offset, at least in part, by the preferential atmospheric escape of Ar relative to CO₂, and by mantle degassing. Based on Mars' elevated ³⁸Ar/³⁶Ar ratio of ~0.24 (Bogard et al., 2001), non-thermal escape processes are estimated to have removed approximately 50% of Mars' atmospheric Ar not lost to space via impact erosion (Jakosky and Phillips, 2001). If we assume no loss of atmospheric CO₂ (to be consistent with the constraints on CO₂ sequestration imposed above), then CO₂ has then been enriched by up to 50% relative to ³⁶Ar. Likewise, planetary degassing enriches the atmosphere in CO₂ as mantle-derived volatiles are depleted in ³⁶Ar relative to the atmosphere (discussed above). In our model, ~2 bars of mantle-derived CO₂ are degassed; the resulting enrichment in CO₂ relative to ³⁶Ar is directly proportional to atmospheric pressure, and is >25% at initial atmospheric pressures as high as 5 bars. Altogether, we expect that increases in the atmospheric ³⁶Ar/(CO₂ + N₂) ratio due to CO₂ sequestration in carbonates (up to 90%) were approximately offset by decreases due to escape processes (up to 50%) and mantle degassing (>25%). Thus we use a primordial atmospheric ³⁶Ar/(CO₂ + N₂) ratio of 10^{-5} in our preferred model, with one log unit uncertainty. Fractionation of N₂ has been ignored because of its low abundance relative to CO₂.

4. Results and discussion

In Fig. 2, using our preferred model parameters (Table 1), we show a selection of linearly and exponentially decreasing paleoatmospheric pressure paths that yield an ⁴⁰Ar/³⁶Ar ratio of 626 ± 100 at 4.16 Ga. A more extensive array of pressure paths that succeed and fail to predict this ratio, along with an analysis of the model sensitivities to each of four variable parameters listed in Table 1, is given in the Supplementary Files. We find that low atmospheric pressures throughout the Noachian (<1 bar on average) are required to produce the observed ⁴⁰Ar/³⁶Ar ratio at 4.16 Ga. Higher atmospheric pressures, and therefore greater total abundances of atmospheric ³⁶Ar, preclude an adequate increase in the ⁴⁰Ar/³⁶Ar ratio for the range in mantle degassing scenarios explored and our best estimates of planetary and atmospheric element abundances. All scenarios require atmospheric pressures of <400 mbar by 4.16 Ga, which implies up to 3.5 bars of atmospheric CO₂ were lost during the first 400 million years of the Noachian (~2 bars of magmatic CO₂ degassed from the mantle through time plus up to 1.5 bars of the initial atmospheric CO₂).

In our model, we assume that the decline in atmospheric pressure is caused solely by impact erosion, which does not fractionate isotopes or chemical species. If, however, CO₂ sequestration into carbonates also drove down atmospheric pressures, then we have overstated the loss of ³⁶Ar by impact erosion and even lower atmospheric pressures are required to predict the ⁴⁰Ar/³⁶Ar ratio of 626 ± 100 at 4.16 Ga. Conversely, if early hydrodynamic escape preferentially removed ³⁶Ar relative to ⁴⁰Ar, then we have understated the loss of ³⁶Ar by impact erosion and greater atmospheric pressures are required. However, nitrogen isotopes in ALH 84001 maskelynite are significantly less fractionated than those in the modern martian atmosphere (Bogard et al., 2001), which suggests that non-thermal escape occurring throughout the past ~4 Ga, not early hydrodynamic escape, may be principally responsible for heavy isotope enrichments. Therefore, because the modern martian atmospheric ³⁸Ar/³⁶Ar ratio is only enriched by 30% relative to the primordial value (Jakosky and Phillips, 2001), our model results would not differ significantly if early hydrodynamic escape were considered. Moreover, if a less voluminous magma production model than Breuer and Spohn (2006) was used, then even lower atmospheric pressures would be required (discussed above).

² Calculated assuming the martian atmosphere contains 1.6% Ar by volume (Owen et al., 1977) with a ⁴⁰Ar/³⁶Ar ratio of 1800 (Bogard et al., 2001).

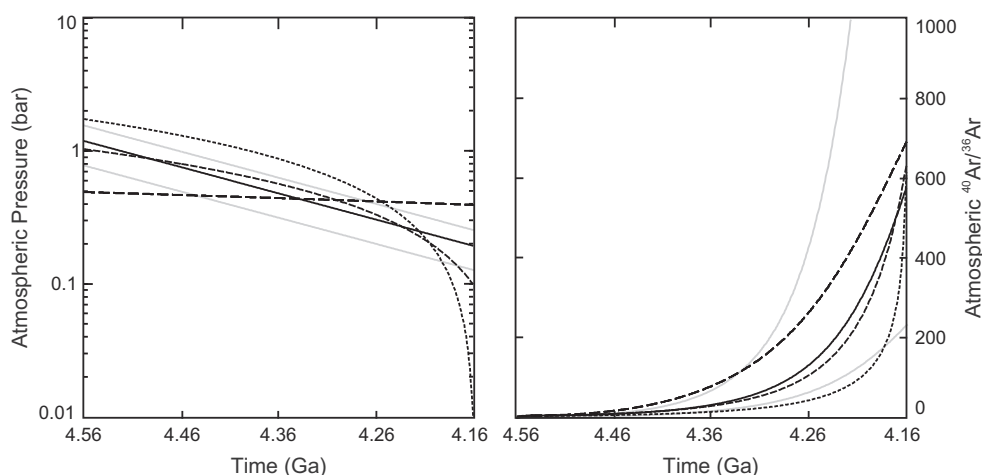


Fig. 2. Modeled paleoatmospheric pressure paths (left) and corresponding evolution in the atmospheric $^{40}\text{Ar}/^{36}\text{Ar}$ ratio (right) for the model parameters listed in Table 1. Dashed curves denote a constant rate of pressure change and solid lines an exponential decrease. Four atmospheric pressure models that predict an $^{40}\text{Ar}/^{36}\text{Ar}$ ratio within 626 ± 100 at 4.16 Ga are shown in black. For comparison, two models that fail to predict this ratio are shown in gray; an array of additional scenarios excluded by the ALH 84001 data is shown in the Supplementary Files. Linearly decreasing pressure paths were forced to evolve to pressures ranging between 10 mbar and 10 bar at 4.16 Ga; those forced to final pressures >400 mbar predict $^{40}\text{Ar}/^{36}\text{Ar}$ ratios less than 626 ± 100 and are therefore excluded. For clarity, only results for final pressures of 10 mbar, 100 mbar, and 400 mbar are shown. Exponential pressure models decline at the same rate as the martian impact flux (Melosh and Vickery, 1989) (see Supplementary Files), with $\sim 16\%$ of the initial pressures at 4.16 Ga. The curves shown in black are representative of the range of permissible linear, exponential, and random solutions (see Fig. S1) and require <1 bar of atmospheric pressure (on average) throughout most of the Noachian. A detailed analysis of the model sensitivity to input parameters is given in the Supplementary Files.

In summary, our model results indicate that atmospheric pressures during the Early to Middle Noachian were likely less than ~ 1 bar. This suggests that a long-lived, CO_2 -based greenhouse atmosphere with surface temperatures above the melting point of H_2O did not exist at that time. The apparent absence of massive carbonate deposits may be consistent with this result. The model results are also consistent with the observation that the formation of phyllosilicates observed in the Noachian crust required low partial pressures of atmospheric CO_2 (Chevrier et al., 2007). Although it is possible that an extended greenhouse climate may have existed after the period of our meteoritic constraint (i.e., after 4.16 Ga), geomorphic and spectral observations indicate that the Noachian was on average the warmest and wettest period on Mars (Bibring et al., 2006; Carr and Head, 2010). Therefore, if the trapped $^{40}\text{Ar}/^{36}\text{Ar}$ ratio observed in ALH 84001 is a sample of the Noachian martian atmosphere, then even during this putative warm period it appears that water was only intermittently stable in the liquid phase.

Impact events or intense volcanism may have caused such intermittent conditions by delivering other greenhouse gases to the atmosphere, such as SO_2 , H_2S , and water vapor (Toon et al., 2010). Given the partial pressures of CO_2 permitted by our model results, temporarily elevated partial pressures of these other atmospheric gases (e.g., $\sim 2 \times 10^{-6}$ bars of SO_2) could have stabilized liquid water on Mars' surface at high latitudes (Halevy et al., 2007; Johnson et al., 2008; Tian et al., 2010). The discovery of sulfate deposits in the martian regolith underscores the potential role of SO_2 and H_2S as greenhouse gases. Even in the absence of such gases, liquid water would be stable at low latitudes during seasonally warm periods given the partial pressures of CO_2 permitted by our model results. Thus, existing observations of surface and meteorite mineralogy, coupled with the trapped Ar component identified in ALH 84001, suggest that the mean Noachian climate on Mars was cool (below freezing) and dry (without liquid water), with only intermittent periods of warm and wet conditions.

Acknowledgments

The authors acknowledge financial support from the NASA Mars Fundamental Research program (Grant MFRP05-0108 to B.P.W. and D.L.S.), the NSF Petrology and Geochemistry program (Grant EAR-0838572 to P.R.R. and D.L.S.), the NSF Major Research Instrumentation program (Grant EAR-0618219 to D.L.S. and P.R.R.), and the Ann and Gordon Getty Foundation. W.S. Cassata was supported by a National Science Foundation Graduate Research Fellowship. W.S. Cassata thanks Michael Manga, Edwin Kite, and Chris Huber for constructive discussions related to this paper.

Appendix A. Supplementary material

Supplementary data associated with this article can be found, in the online version, at <http://dx.doi.org/10.1016/j.icarus.2012.05.005>.

References

- Anders, E., Owen, T., 1977. Mars and Earth: Origin and abundance of volatiles. *Science* 198, 453–465.
- Arvidson, R.E. et al., 2005. Spectral reflectance and morphologic correlations in eastern Terra Meridiani, Mars. *Science* 307, 1591–1594.
- Bandfield, J.L., 2002. Global mineral distributions on Mars. *J. Geophys. Res. E: Planets* 107, 1–9.
- Begemann, F., Weber, H.W., Hintenberger, H., 1976. On the primordial abundance of argon-40. *Astrophys. J.* 203, L155–L157.
- Bibring, J.P. et al., 2006. Global mineralogical and aqueous Mars history derived from OMEGA/Mars Express data. *Science* 312, 400–404.
- Boctor, N.Z., Wang, J., Alexander, C.M., Hauri, E., Irving, A.J., 2005. Volatile abundances in minerals and glasses from the Nakhilites and the Shergottite Zagami. In: 68th Annual Meteoritical Society Meeting, p. 5261.
- Boctor, N.Z., Wang, J., Alexander, C.M., Hauri, E., 2006. Volatile abundances and H isotope signatures of melt inclusions and nominally anhydrous minerals in the chassignites and ALH84001. In: 37th Annual Lunar and Planetary Science Conference, p. 1412.
- Bogard, D.D., Clayton, R.N., Marti, K., Owen, T., Turner, G., 2001. Martian volatiles: Isotopic composition, origin, and evolution. *Space Sci. Rev.* 96, 425–458.
- Bouvier, V., Blichert-Toft, J., Albarède, F., 2009. Martian meteorite chronology and the evolution of the interior of Mars. *Earth Planet. Sci. Lett.* 280, 285–295.
- Boynton, W.V. et al., 2009. Evidence for calcium carbonate at the Mars Phoenix landing site. *Science* 325, 61–64.
- Brain, D.A., Jakosky, B.M., 1998. Atmospheric loss since the onset of the martian geologic record: Combined role of impact erosion and sputtering. *J. Geophys. Res.* 103, 22689–22694.
- Breuer, D., Spohn, T., 2006. Viscosity of the martian mantle and its initial temperature: Constraints from crust formation history and the evolution of the magnetic field. *Planet. Space Sci.* 54, 153–169.
- Carr, M.H., Head, J.W., 2010. Geologic history of Mars. *Earth Planet. Sci. Lett.* 294, 185–203.
- Cassata, W.S., Shuster, D.L., Renne, P.R., Weiss, B.P., 2010. Evidence for shock heating and constraints on martian surface temperatures revealed by $^{40}\text{Ar}/^{39}\text{Ar}$ thermochronometry of martian meteorites. *Geochim. Cosmochim. Acta* 74, 6900–6920.
- Catling, D.C., Leovy, C., 2007. Mars atmosphere: History and surface interactions. In: Lucy-Ann McFadden et al. (Eds.), *Encyclopedia of the Solar System*, pp. 301–314.
- Chevrier, V., Poulet, F., Bibring, J.P., 2007. Early geochemical environment of Mars as determined from thermodynamics of phyllosilicates. *Nature* 448, 60–63.
- Christensen, P.R. et al., 2004. Initial results from the Mini-TES experiment in Gusev Crater from the Spirit Rover. *Science* 305, 837–842.
- Colaprete, A., Toon, O.B., 2003. Carbon dioxide clouds in an early dense martian atmosphere. *J. Geophys. Res.* 108, 1–6.
- Donahue, T.M., Pollack, J.B., 1983. Origin and evolution of the atmosphere of Venus. *Venus. University of Arizona Press, Tucson*, pp. 1003–1036.
- Dreibus, G. et al., 1982. *Lunar Planet. Sci. Conf. XIII*, 13, 186–187.

- Gendrin, A. et al., 2005. Sulfates in martian layered terrains: The OMEGA/Mars Express view. *Science* 307, 1587–1591.
- Halevy, I., Zuber, M.T., Schrag, D.P., 2007. A sulfur dioxide climate feedback on early Mars. *Science* 318, 1903–1907.
- Hirschmann, M.M., Withers, A.C., 2008. Ventilation of CO₂ from a reduced mantle and consequences for the early martian greenhouse. *Earth Planet. Sci. Lett.* 270, 147–155.
- Hutchins, K.S., Jakosky, B.M., Luhmann, J.G., 1997. Impact of a paleomagnetic field on sputtering loss of martian atmospheric argon and neon. *J. Geophys. Res.* 102, 9183–9189.
- Jakosky, B.M., Phillips, R.J., 2001. Mars' volatile and climate history. *Nature* 412, 237–244.
- Johnson, S.S., Mischna, M.A., Grove, T.L., Zuber, M.T., 2008. Sulfur-induced greenhouse warming on early Mars. *J. Geophys. Res.* 113, E08005.
- Lapen, T. et al., 2010. A younger age for ALH84001 and its geochemical link to shergottite sources in Mars. *Science* 328, 347–351.
- Lee, J.Y. et al., 2006. A redetermination of the isotopic abundances of atmospheric Ar. *Geochim. Cosmochim. Acta* 70, 4507–4512.
- Lodders, K., Fegley, B., 1997. An oxygen isotope model for the composition of Mars. *Icarus* 126, 373–394.
- Manning, C.V., McKay, C.P., Zahnle, K.J., 2006. Thick and thin models of the evolution of carbon dioxide on Mars. *Icarus* 180, 38–59.
- McDonough, W.F., Sun, S.S., 1995. The composition of the Earth. *Chem. Geol.* 120, 223–253.
- Melosh, H.J., Vickery, A.M., 1989. Impact erosion of the primordial atmosphere of Mars. *Nature* 338, 487–489.
- Michalski, J.R., Niles, P.B., 2010. Deep crustal carbonate rocks exposed by meteor impact on Mars. *Nat. Geosci.* 3, 751–755.
- Morris, R.V. et al., 2010. Identification of carbonate-rich outcrops on Mars by the Spirit Rover. *Science* 329, 421–424.
- Murchie, S.L. et al., 2009. A synthesis of martian aqueous mineralogy after 1 Mars year of observations from the Mars Reconnaissance Orbiter. *J. Geophys. Res.* 114, 1–30. doi:10.1029/2009JE003342.
- Neukum, G., Wise, D.U., 1976. Mars – A standard crater curve and possible new time scale. *Science* 194, 1381–1387.
- Owen, T., Bar-Nun, A., 1995. Comets, impacts, and atmospheres. *Icarus* 116, 215–226.
- Owen, T. et al., 1977. The composition of the atmosphere at the surface of Mars. *J. Geophys. Res.* 82, 4635–4639.
- Pepin, R.O., 1994. Evolution of the martian atmosphere. *Icarus* 111, 289–304.
- Pollack, J.B., Kasting, J.F., Richardson, S.M., Poliakov, K., 1987. The case for a wet, warm climate on early Mars. *Icarus* 71, 203–224.
- Roberts, J.H., Lillis, R.J., Manga, M., 2009. Giant impacts on early Mars and the cessation of the martian dynamo. *J. Geophys. Res.* 114. doi:10.1029/2008JE003287.
- Saal, A.E., Hauri, E.H., Langmuir, C.H., Perfit, M.R., 2002. Vapour undersaturation in primitive mid-ocean-ridge basalt and the volatile content of Earth's upper mantle. *Nature* 419, 451–455.
- Segura, T.L., Toon, O.B., Colaprete, A., Zahnle, K., 2002. Environmental effects of large impacts on Mars. *Science* 298, 1977–1980.
- Sohl, F., Spohn, T., 1997. The interior structure of Mars: Implications from SNC meteorites. *J. Geophys. Res.* 102, 1613–1635.
- Squyres, S.W. et al., 2004. In situ evidence for an ancient aqueous environment at Meridiani Planum, Mars. *Science* 306, 1709–1714.
- Taylor, G.J. et al., 2006. Bulk composition and early differentiation of Mars. *J. Geophys. Res.* 111, E03S10.
- Tian, F. et al., 2010. Photochemical and climate consequences of sulfur outgassing on early Mars. *Earth Planet. Sci. Lett.* 295, 412–418.
- Toon, O.B., Segura, T., Zahnle, K., 2010. The formation of martian river valleys by impacts. *Annu. Rev. Earth Planet. Sci.* 38, 303–322.
- Weiss, B.P., Fong, L.E., Vali, H., Lima, E.A., Baudenbacher, F.J., 2008. Paleointensity of the ancient martian magnetic field. *Geophys. Res. Lett.* 35, L23207.
- Yung, Y.L., Nair, H., Gerstell, M.F., 1997. CO₂ greenhouse in the early martian atmosphere: SO₂ inhibits condensation. *Icarus* 130, 222–224.
- Zehring, J., 1966. Primordial argon and the metamorphism of chondrites. *Earth Planet. Sci. Lett.* 1, 379–382.

Supplementary Files for:

Trapped Ar isotopes in meteorite ALH 84001 indicate Mars did not have a thick ancient atmosphere

William S. Cassata^{1,2,*}, David L. Shuster^{1,2}, Paul R. Renne^{1,2}, Benjamin P. Weiss³

1. Department of Earth and Planetary Science, University of California - Berkeley, 307 McCone Hall #4767, Berkeley, CA 94720-4767, USA (cassata@berkeley.edu)
2. Berkeley Geochronology Center, 2455 Ridge Road, Berkeley, CA 94709, USA (prenne@bgc.org, dshuster@bgc.org)
3. Department of Earth, Atmospheric, and Planetary Sciences, Massachusetts Institute of Technology, 77 Massachusetts Avenue, Cambridge, MA 02139, USA (bpweiss@mit.edu)

* Corresponding author

Contents:

Supplementary Discussions:

Discussion S1: Calculation details

Discussion S2: The origin of trapped Ar in ALH 84001

Supplementary References

Supplementary Figures

Fig. S1: Illustration of the range of paleoatmospheric pressure paths explored.

Fig. S2: Illustration of the model sensitivity to the K concentration of extracted magmas.

Fig. S3: Illustration of the model sensitivity to the CO₂ and N₂ concentration of extracted magmas.

Fig. S4: Illustration of the model sensitivity to the ³⁶Ar concentration of extracted magmas.

Fig. S5: Illustration of the model sensitivity to the primordial concentration of atmospheric ³⁶Ar.

Supplementary Tables

Table S1: ⁴⁰Ar/³⁶Ar ratios of trapped components identified in ALH 84001, Nakhla, and MIL 03346.

Discussion S1: Calculation Details

The generalized equation describing the atmospheric molar abundance of isotope X is given by

$$\frac{d^X Ar}{dt} = N_X(t) - \left({}^X Ar \frac{L(t)}{P(t)} \right). \quad (\text{Eq. S1})$$

In this section we define each term in Eq. (S1) and discuss our discretized implementation. A complete list of variables and the range of values explored can be found in Table 1.

i.) ${}^X Ar$ is the atmospheric abundance of isotope X in moles or atoms.

At all $t > t_0$, ${}^X Ar$ reflects the integrated effects of production and loss. At t_0 , the mass of atmospheric ${}^{36}\text{Ar}$ is given by

$$m_{36_0} = \frac{R_{atm} \cdot P_0 \cdot 4\pi r^2}{g} \quad (\text{Eq. S2})$$

where P_0 is total atmospheric pressure at t_0 , g is the gravitational constant (3.72 m/s^2), r is the radius of Mars ($3397 \times 10^3 \text{ m}$), and R_{atm} is the atmospheric ${}^{36}\text{Ar}/(\text{CO}_2 + \text{N}_2)$ ratio (i.e., the fractional abundance of atmospheric ${}^{36}\text{Ar}$). P_0 is a free parameter that is defined by hypothetical paleoatmospheric pressure paths. The molar abundance of atmospheric ${}^{40}\text{Ar}$ at t_0 is simply 10^{-3} times the molar abundance of atmospheric ${}^{36}\text{Ar}$ (Begemann et al., 1976).

ii.) $N_X(t)$ is the rate of addition of isotope X to the atmosphere as a function of time due asteroid accretion and planetary degassing.

Asteroid Accretion:

To model the mass of ^{40}Ar added to the atmosphere by asteroids, we use the Martian impact flux derived by Melosh and Vickery (1989) from the lunar cratering record of Neukum and Wise (1976) following Manning et al. (2006), given by

$$m_{\text{asteroid}}(t) = 6.85 * 10^{12} \left(1 + 2300 e^{-\left(\frac{10^3 * (4.56 - t)}{220} \right)} \right) \left(\frac{\text{kg}}{\text{Ma}} \right) \quad (\text{Eq. S3})$$

where m_{asteroid} is the mass of asteroid material and t is time ranging from 4.56 to 4.16 Ga. The amount of asteroid-derived ^{40}Ar is given by

$$^{40}\text{Ar}(t) = ^{40}K_a \frac{\lambda_e}{\lambda} \left(e^{-\lambda(4.56 - t)} \right) \quad (\text{Eq. S4})$$

where $^{40}K_a$ is moles of ^{40}K in a given mass of asteroid material, λ_e is the partial decay constant for electron capture ($0.576 \times 10^{-1} \text{ Ga}^{-1}$) (Renne et al., 2011), and λ is the total decay constant ($5.531 \times 10^{-1} \text{ Ga}^{-1}$) (Renne et al., 2011). We assume that impacting asteroids contain a chondritic abundance of K (550 ppm; McDonough and Sun, 1995) and ^{36}Ar concentrations typical of H-, L-, and LL-chondrites (~ 15 ppt; Zahringer, 1966).

Planetary degassing:

To model the production of atmospheric volatiles associated with surface, crustal, and upper mantle magmatic activity, we use the crustal production model of Breuer and Spohn (2006), approximated between 4.56 and 4.16 Ga by the following expression:

$$V_{\text{magma}}(t) = \left[\left(1.7075 * 10^3 \right) t^3 - \left(2.1989 * 10^4 \right) t^2 + \left(9.4408 * 10^4 \right) t - \left(1.3512 * 10^5 \right) \right] \frac{\text{km}^3}{\text{a}} \quad (\text{Eq. S5})$$

where t is time ranging from 4.56 to 4.16 Ga.

The mass of mantle-derived ^{36}Ar is given by

$$m_{^{36}\text{magma}}(t) = V_{\text{magma}}(t) \rho_{\text{magma}} [\text{CN}]_{\text{magma}} R_{\text{magma}} \quad (\text{Eq. S6})$$

where ρ_{magma} is the magma density (3000 kg/m³), $[CN]_{\text{magma}}$ is the magmatic concentration of N₂ + CO₂, and R_{magma} is the magmatic ³⁶Ar/(CO₂ + N₂) ratio.

The molar production of ⁴⁰Ar is given by

$$^{40}\text{Ar}(t) = ^{40}\text{K}_m \frac{\lambda_\epsilon}{\lambda} \left(e^{-\lambda(4.56-t)} \right) \quad (\text{Eq. S7})$$

where $^{40}\text{K}_m$ is moles of ⁴⁰K in a given volume of magma. We modeled scenarios in which magmas contain between 1300 and 3300 ppm K (Table 1).

iii.) $\frac{L(t)}{P(t)}$ is the fractional loss rate of atmospheric gases due to impact erosion, which we assume does not

fractionate isotopes or chemical species (Brain and Jakosky, 1998; Melosh and Vickery, 1989).

$P(t)$ is atmospheric pressure (defined by the hypothetical paleoatmospheric pressure paths) and $L(t)$ is the atmospheric pressure loss rate due to impact erosion, derived from the following equation:

$$\frac{dP}{dt} = I(t) - L(t), \quad (\text{Eq. S8})$$

where $I(t)$ is the rate of increase in atmospheric pressure resulting from planetary degassing, given by the following equation:

$$I(t) = \frac{V_{\text{magma}}(t) \rho_{\text{magma}} [CN]_{\text{magma}} g \text{ bar}}{4\pi r^2 \text{ Ma}}. \quad (\text{Eq. S9})$$

Thus $L(t)$ can be extracted from the discretized version of equation Eq. (S8), given by

$$P(t) = P(t-dt) + dt(-L(t) + I(t)), \quad (\text{Eq. S10})$$

where $P(t)$ and $P(t-dt)$ are two points on a hypothetical paleoatmospheric pressure path.

The discretized version of Eq. (S1) is then solved for both ^{40}Ar and ^{36}Ar according to the following:

$$^x\text{Ar}(t) = \left(1 + dt \frac{L(t)}{P(t)}\right)^{-1} \left(^x\text{Ar}(t - dt) + dt N_x(t)\right). \quad (\text{Eq. S11})$$

Discussion S2: The origin of trapped Ar in ALH 84001

Critical to our argument is the assumption that the trapped argon component identified within maskelynite in ALH 84001 is atmospheric in origin and that it was acquired at 4.16 Ga. Although Xe isotopes in ALH 84001 confirm that atmospheric gas is present (Mathew et al., 1998; Swindle et al., 1995), it is conceivable that the $^{40}\text{Ar}/^{36}\text{Ar}$ ratio of trapped gas within maskelynite (i) is contaminated by a mantle Ar component, (ii) is contaminated by a non-atmospheric upper crustal Ar component, or (iii) reflects a post-crystallization shock-implemented Ar component. We find these possibilities unlikely for reasons discussed below.

i.) A mantle Ar component

Argon is highly mobile in feldspars at temperatures as low as 300-400 °C (Cassata et al., 2009). As such, feldspars should continue to exchange Ar with the local environment during near-surface cooling, and are not expected to retain the isotopic composition of Ar in primary melts extracted from the Martian mantle, which have temperatures in excess of 1200 °C.

ii.) An upper crustal Ar component

Crystals generally incorporate excess argon as a result of (1) thermally-induced in-diffusion of grain boundary ^{40}Ar or (2) growth within magmas and interaction with fluids characterized by supra-atmospheric $^{40}\text{Ar}/^{36}\text{Ar}$ ratios. Given that three separate whole-rock fragments of ALH 84001 that each have different local maskelynite grain boundary environments and different grain size distributions yield indistinguishable trapped $^{40}\text{Ar}/^{36}\text{Ar}$ ratios (Table S1), we consider it probable that maskelynite (or the precursor feldspar) equilibrated within a uniform Ar reservoir. When rocks are subjected to high a Ar pressure and an elevated $^{40}\text{Ar}/^{36}\text{Ar}$ ratio produced by degassing of old, K-rich phases such as occurs in contact metamorphic aureoles (Harrison and McDougall, 1981; Renne et al., 1990) or in intrusions near such aureoles (Lanphere and Brent Dalrymple, 1976; Marzoli et al., 1999), the trapped “excess” ^{40}Ar component is generally manifest in step-heating experiments by anomalously high apparent ages derived from low temperature steps, which typically decrease with increasing extraction temperature. This implies a decreasing proportion of trapped relative to radiogenic Ar components, generally interpreted as being due to some combination of the trapped component being (i) surface-correlated, i.e. through inward diffusion, and (ii) sited in vacancies or microfractures with low activation energies (Harrison and McDougall, 1981). Thus post-crystallization in-diffusion of grain-boundary ^{40}Ar from degassing country rocks can be dismissed as a plausible source of Ar, as one would expect the trapped $^{40}\text{Ar}/^{36}\text{Ar}$ ratio to be spatially variable.

If the trapped component observed in maskelynite reflects a uniformly distributed supra-atmospheric component, then the evolved parental magma to ALH 84001 must have incorporated and homogenized excess ^{40}Ar from upper crustal rocks, possibly through interactions with crustal groundwater and pore gases. Such a scenario seems unlikely, as the trapped $^{40}\text{Ar}/^{36}\text{Ar}$ ratios observed in petrogenetically similar feldspathic phases in Shergottites and Nakhilites (Table S1) do not exceed the inferred atmospheric value of ~ 1800 (Bogard et al., 2001; Cassata et al., 2010). Moreover, in our experience, such cases of feldspar and glass contamination with argon having an appreciably (e.g., $>20\%$) supra-atmospheric $^{40}\text{Ar}/^{36}\text{Ar}$ ratio generally fail to produce well-defined isochrons because the trapped component is not isotopically

homogeneous. Trapped components of Ar in terrestrial plagioclase, in both extrusive and intrusive rocks, commonly have atmospheric $^{40}\text{Ar}/^{36}\text{Ar}$ compositions as indicated in flat apparent age spectra (Ernesto et al., 1999; Renne et al., 1996) wherein apparent ages are computed using an air correction.

iii.) A post-4.16 Ga shock-implanted Ar component

ALH 84001 appears to have been subjected to a significant shock event at ~ 1 Ga wherein both maskelynite and pyroxenes were locally heated to high temperatures, resulting in Ar loss (Cassata et al., 2010). Bogard et al. (1986) showed that unfractionated noble gases can be incorporated into crystals during such shock events. If the trapped $^{40}\text{Ar}/^{36}\text{Ar}$ ratio observed within maskelynite reflects shock implanted atmospheric Ar associated with the ~ 1 Ga event, then by implication the Martian atmospheric $^{40}\text{Ar}/^{36}\text{Ar}$ ratio at ~ 1 Ga was ~ 600 . However, the ~ 1.3 Ga Martian meteorites MIL 03346 and Nakhla yield a weighted average trapped $^{40}\text{Ar}/^{36}\text{Ar}$ ratio of 1600 ± 200 , which suggests the Martian atmospheric $^{40}\text{Ar}/^{36}\text{Ar}$ ratio at ~ 1 Ga was much greater than 600 (Table S1; Cassata et al., 2010). If the trapped $^{40}\text{Ar}/^{36}\text{Ar}$ reflects shock implanted Ar associated with a hitherto unrecognized shock event that occurred between 4.16 Ga and ~ 1 Ga, then it must have been implanted without disturbance to the distribution of radiogenic ^{40}Ar (see plateau in ALH-1 from Cassata et al., 2010), which requires shock pressures lower than 10-15 GPa (Bogard et al., 1988). At these low pressures, the implantation efficiency of atmospheric gases is greatly reduced (Bogard et al., 1986), and those gases that are implanted are degassed at low temperatures (i.e., they are surface correlated or contained within microfractures; Bogard et al., 1986). In ALH 84001, the trapped Ar component is pervasive, comprising more than 10% of the total ^{40}Ar in the highest temperature maskelynite extractions (see Cassata et al., 2010). As such, we find it unlikely that a minor shock event between 4.16 and ~ 1 Ga implanted the observed trapped component.

We hold that the simplest explanation for the trapping of Ar isotopes observed within maskelynite in ALH 84001 is equilibration with a near-atmospheric reservoir at 4.16 Ga.

Supplementary References

- Begemann, F., Weber, H.W., Hintenberger, H., 1976. On the primordial abundance of argon-40. *Astrophys. J.* 203.
- Bogard, D., Horz, F., Stoffler, D., 1988. Loss of radiogenic argon from shocked granitic clasts in suevite deposits from the Ries Crater. *Geochimica et Cosmochimica Acta* 52, 2639-2649.
- Bogard, D.D., Clayton, R.N., Marti, K., Owen, T., Turner, G., 2001. Martian volatiles: isotopic composition, origin, and evolution. *Space Science Reviews* 96, 425-458.
- Bogard, D.D., Horz, F., Johnson, P.H., 1986. Shock-implanted noble gases: An experimental study with implications for the origin of Martian gases in shergottite meteorites, 7th Lunar and Planetary Science Conference. *Journal of Geophysical Research*, pp. 99-114.
- Brain, D.A., Jakosky, B.M., 1998. Atmospheric loss since the onset of the Martian geologic record: Combined role of impact erosion and sputtering. *Journal of Geophysical Research* 103, 22689-22694.
- Breuer, D., Spohn, T., 2006. Viscosity of the Martian mantle and its initial temperature: Constraints from crust formation history and the evolution of the magnetic field. *Planetary and Space Science* 54, 153-169.
- Cassata, W.S., Renne, P.R., Shuster, D.L., 2009. Argon diffusion in plagioclase and implications for thermochronometry: A case study from the Bushveld Complex, South Africa. *Geochimica et Cosmochimica Acta* 73, 6600-6612.
- Cassata, W.S., Shuster, D.L., Renne, P.R., Weiss, B.P., 2010. Evidence for shock heating and constraints on Martian surface temperatures revealed by $^{40}\text{Ar}/^{39}\text{Ar}$ thermochronometry of Martian meteorites. *Geochimica et Cosmochimica Acta* 74, 6900-6920.
- Ernesto, M., Raposo, M.I.B., Marques, L.S., Renne, P.R., Diogo, L.A., de Min, A., 1999. Paleomagnetism, geochemistry and $\text{Ar-40}/\text{Ar-39}$ dating of the North-eastern Parana Magmatic Province: tectonic implications. *Journal of Geodynamics* 28, 321-340.
- Harrison, T.M., McDougall, I., 1981. Excess ^{40}Ar in metamorphic rocks from Broken Hill, New South Wales: implications for $^{40}\text{Ar}/^{39}\text{Ar}$ age spectra and the thermal history of the region. *Earth and Planetary Science Letters* 55, 123-149.
- Lanphere, M.A., Brent Dalrymple, G., 1976. Identification of excess ^{40}Ar by the $^{40}\text{Ar}/^{39}\text{Ar}$ age spectrum technique. *Earth and Planetary Science Letters* 32, 141-148.
- Manning, C.V., McKay, C.P., Zahnle, K.J., 2006. Thick and thin models of the evolution of carbon dioxide on Mars. *Icarus* 180, 38-59.
- Marzoli, A., Renne, P.R., Piccirillo, E.M., Ernesto, M., Bellieni, G., De Min, A., 1999. Extensive 200-million-year-old continental flood basalts of the Central Atlantic Magmatic Province. *Science* 284, 616-618.
- Mathew, K., Kim, J., Marti, K., 1998. Martian atmospheric and indigenous components of xenon and nitrogen in the Shergotty, Nakhla, and Chassigny group meteorites. *Meteoritics & Planetary Science* 33, 655-664.

- McDonough, W.F., Sun, S.S., 1995. The composition of the Earth. *Chemical Geology* 120, 223-253.
- Melosh, H.J., Vickery, A.M., 1989. Impact erosion of the primordial atmosphere of Mars. *Nature* 338, 487-489.
- Neukum, G., Wise, D.U., 1976. Mars-A standard crater curve and possible new time scale. *Science* 194, 1381-1387.
- Renne, P.R., Balco, G., Ludwig, K., Mundil, R., Min, K., 2011. Response to the Comment by W. H. Schwarz et al. on "Joint determination of ^{40}K decay constants and $^{40}\text{Ar}^*/^{40}\text{K}$ for the Fish Canyon sanidine standard, and improved accuracy for $^{40}\text{Ar}/^{39}\text{Ar}$ geochronology" by P.R. Renne et al. (2010). *Geochimica et Cosmochimica Acta*.
- Renne, P.R., Deckart, K., Ernesto, M., Feraud, G., Piccirillo, E.M., 1996. Age of the Ponta Grossa dike swarm (Brazil), and implications to Parana flood volcanism. *Earth and Planetary Science Letters* 144, 199-211.
- Renne, P.R., Onstott, T.C., D'Agrella-Filho, M.S., Pacca, I.G., Teixeira, W., 1990. $^{40}\text{Ar}/^{39}\text{Ar}$ dating of 1.0-1.1 Ga magnetizations from the São Francisco and Kalahari cratons: tectonic implications for Pan-African and Brasiliano mobile belts. *Earth and Planetary Science Letters* 101, 349-366.
- Swindle, T., Grier, J., Burkland, M., 1995. Noble gases in orthopyroxenite ALH84001: A different kind of martian meteorite with an atmospheric signature. *Geochimica et Cosmochimica Acta* 59, 793-801.
- Zähringer, J., 1966. Primordial argon and the metamorphism of chondrites. *Earth and Planetary Science Letters* 1, 379-382.

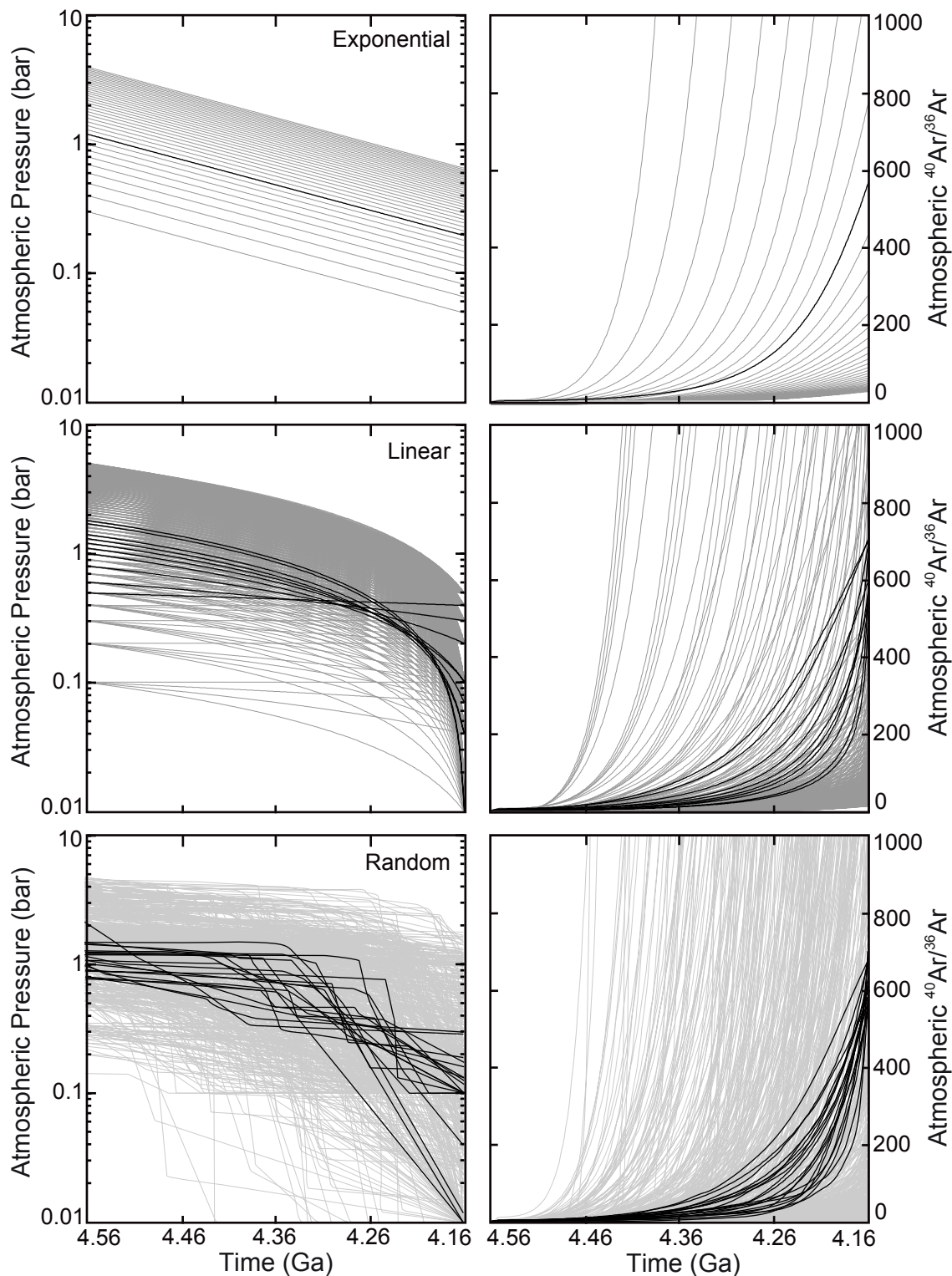


Figure S1: Modeled paleoatmospheric pressure paths (left) and the corresponding evolution in the atmospheric $^{40}\text{Ar}/^{36}\text{Ar}$ ratio (right) for the model parameters listed in Table 1. Atmospheric pressure models that predict an $^{40}\text{Ar}/^{36}\text{Ar}$ ratio within 626 ± 100 at 4.16 Ga are shown in black, and those that do not are shown in gray. Linearly decreasing models (middle) were forced to pressures of 10 mbar to 10 bar at 4.16 Ga; those forced to >400 mbar at 4.16 Ga predict $^{40}\text{Ar}/^{36}\text{Ar}$ ratios lower than 626 ± 100 and are therefore excluded by the ALH 84001 data. Exponential pressure models (upper) decline at the same rate as the Martian impact flux (see text for details), with $\sim 16\%$ of the initial pressures at 4.16 Ga. Random pressure paths (lower) are well approximated by the linear and exponential models. The permissible solutions (shown in black) indicate that low atmospheric pressures (<1 bar on average) prevailed throughout the Early Noachian. In subsequent figures, only the results for exponential paths and linear paths with final pressure of 10 mbar and 100 mbar are shown.

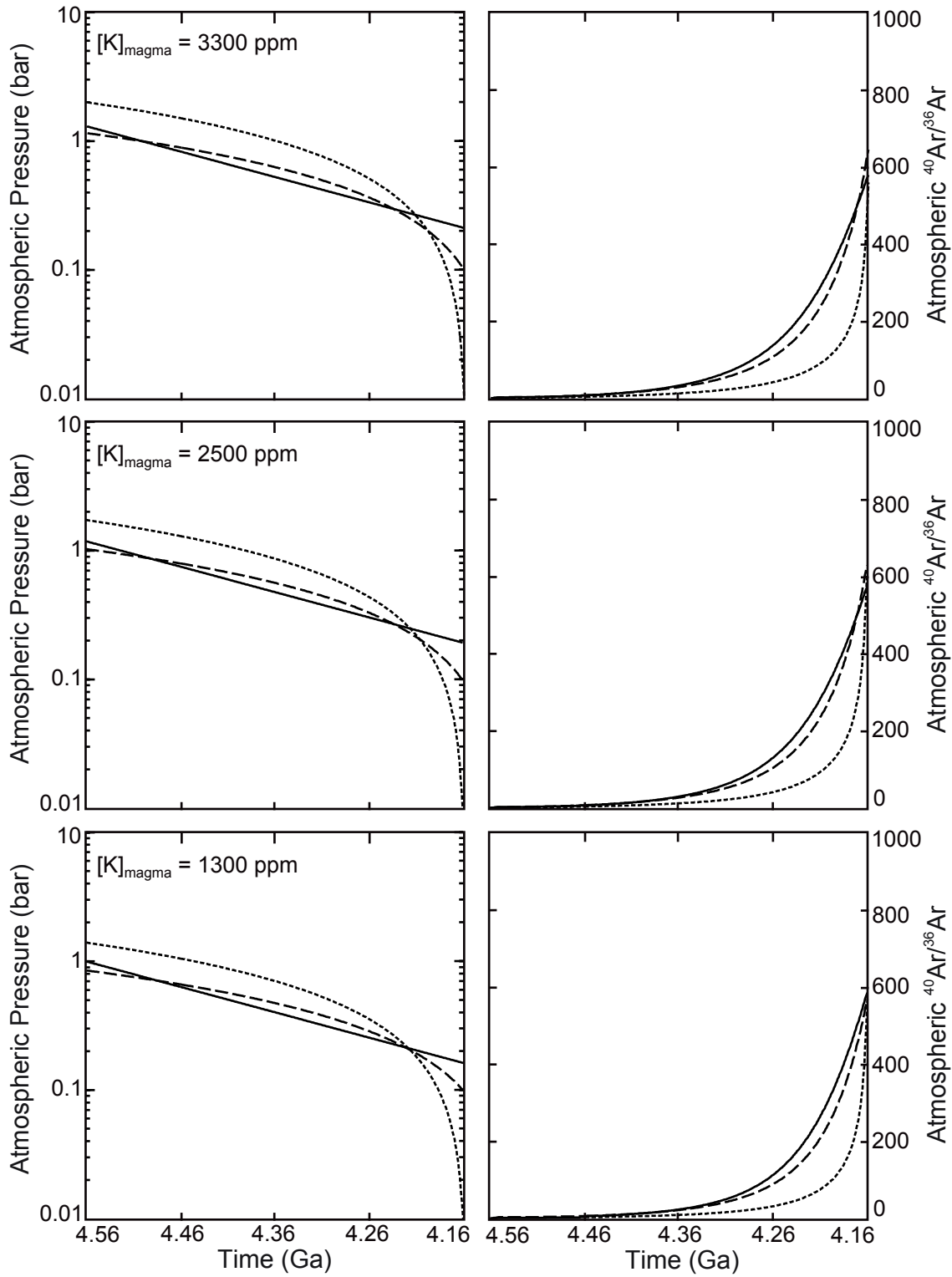


Figure S2: Illustration of the model sensitivity to the K concentration of extracted magmas. Magmas with higher concentrations of K, and therefore ^{40}Ar , more efficiently elevate the atmospheric $^{40}\text{Ar}/^{36}\text{Ar}$ ratio. Thus higher atmospheric pressures (i.e., more atmospheric ^{36}Ar) are required to maintain a given $^{40}\text{Ar}/^{36}\text{Ar}$ ratio if the magmatic K concentration is raised, and vice versa. The center panels represents our preferred model (modified from Fig. 2 in the main text), wherein the K concentration is 2500 ppm.

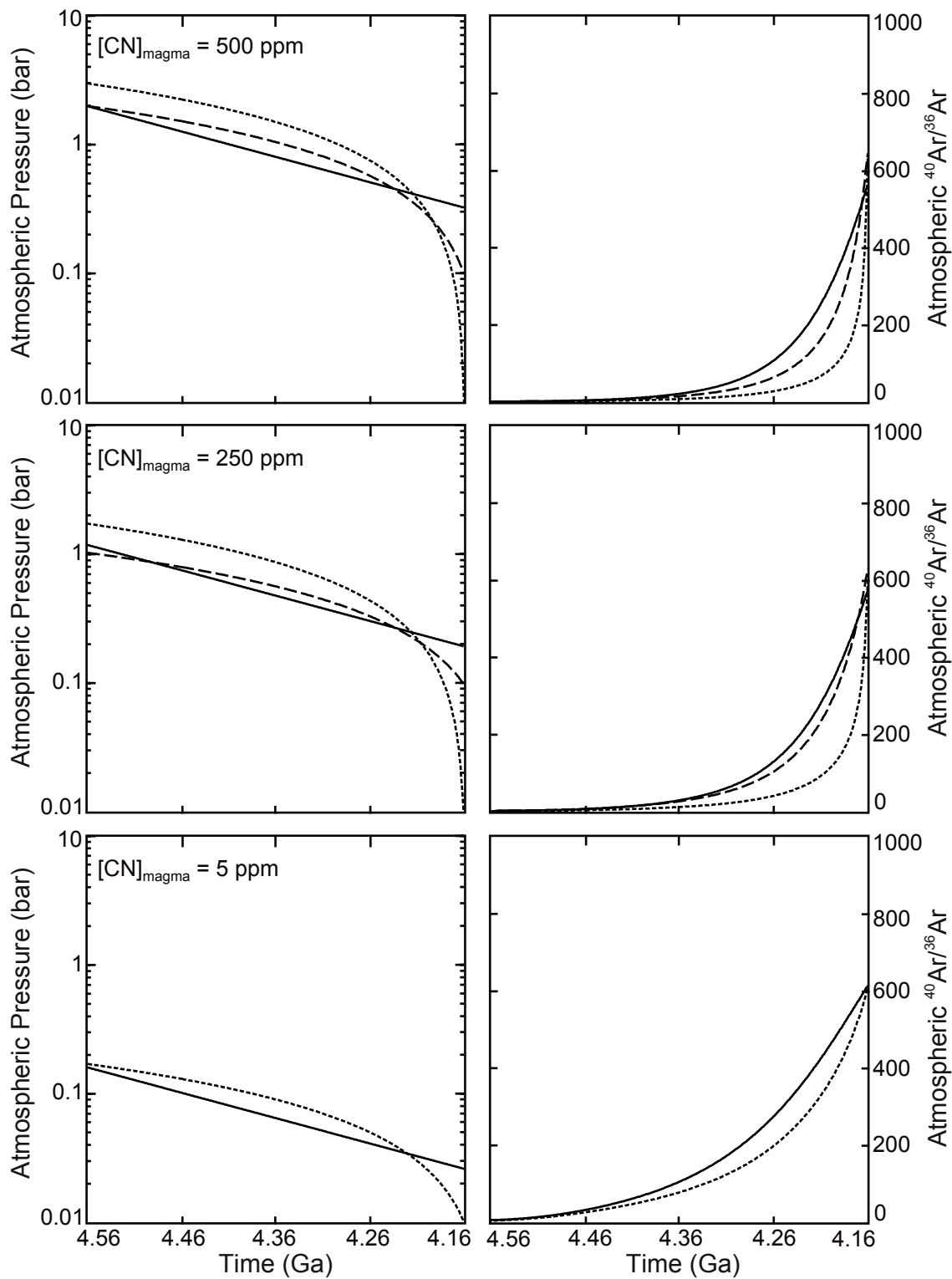


Figure S3: Illustration of the model sensitivity to the CO_2 and N_2 concentration of extracted magmas. Because magmatic $^{36}\text{Ar}/(\text{CO}_2 + \text{N}_2)$ ratios are lower than that of the primordial atmosphere (see text for discussion), magmas with higher concentrations of CO_2 and N_2 more efficiently dilute the concentration of atmospheric ^{36}Ar . Thus higher atmospheric pressures (i.e., more primordial atmospheric ^{36}Ar) are required to maintain a given $^{40}\text{Ar}/^{36}\text{Ar}$ if the magmatic concentrations of CO_2 and N_2 are raised, and vice versa. The center panels represents our preferred model (modified from Fig. 2 in the main text), wherein $[\text{CN}]_{\text{magma}}$ is 250 ppm.

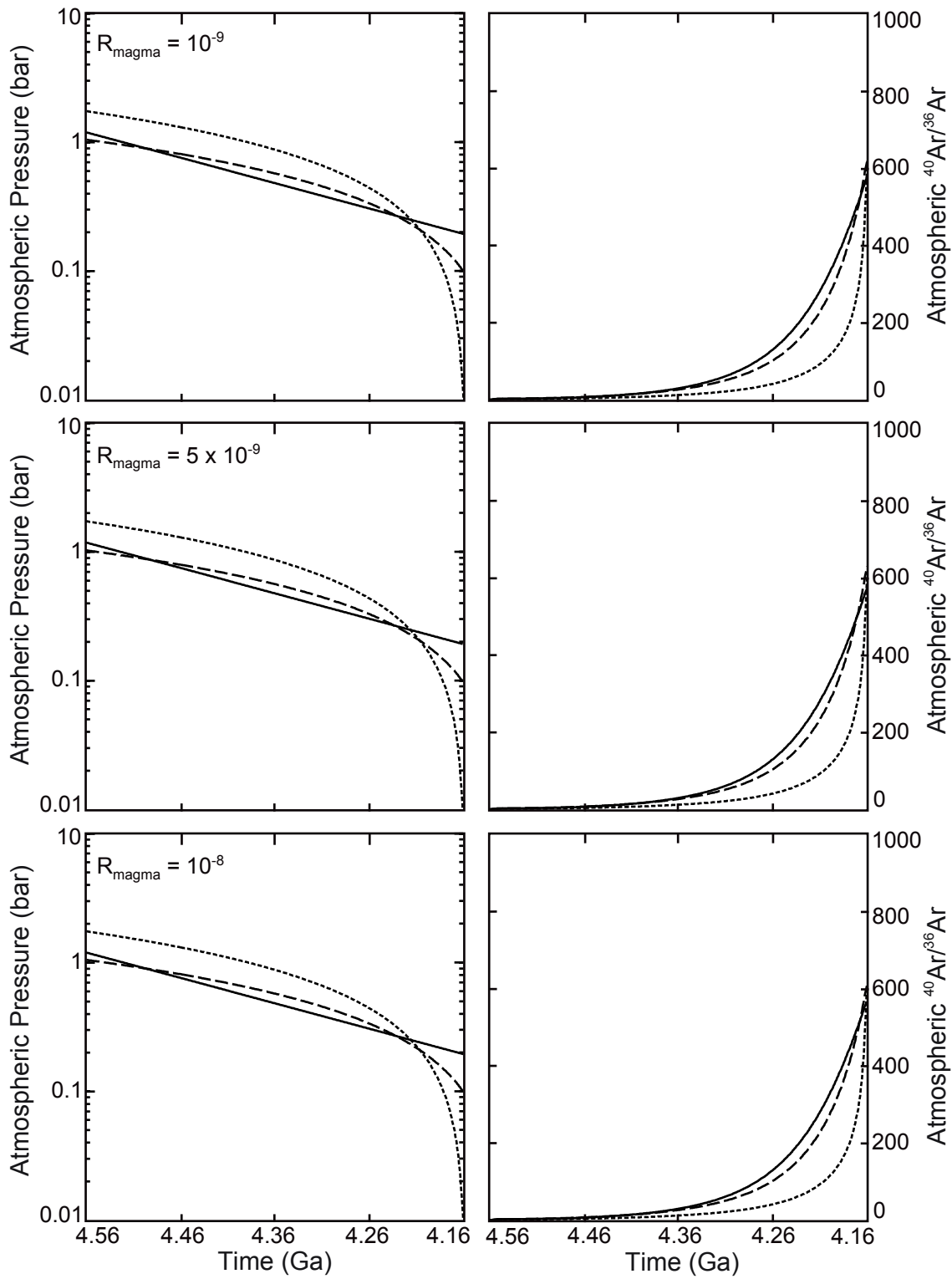


Figure S4: Illustration of the model sensitivity to the ^{36}Ar concentration of extracted magmas. Magmas with lower concentrations of ^{36}Ar more efficiently elevate the atmospheric $^{40}\text{Ar}/^{36}\text{Ar}$ ratio. Thus higher atmospheric pressures (i.e., more atmospheric ^{36}Ar) are required to maintain a given $^{40}\text{Ar}/^{36}\text{Ar}$ ratio if the magmatic concentration of ^{36}Ar is lowered, and vice versa. The center panels represents our preferred model (modified from Fig. 2 in the main text), wherein $[\text{CN}]_{\text{magma}}$ is 250 ppm.

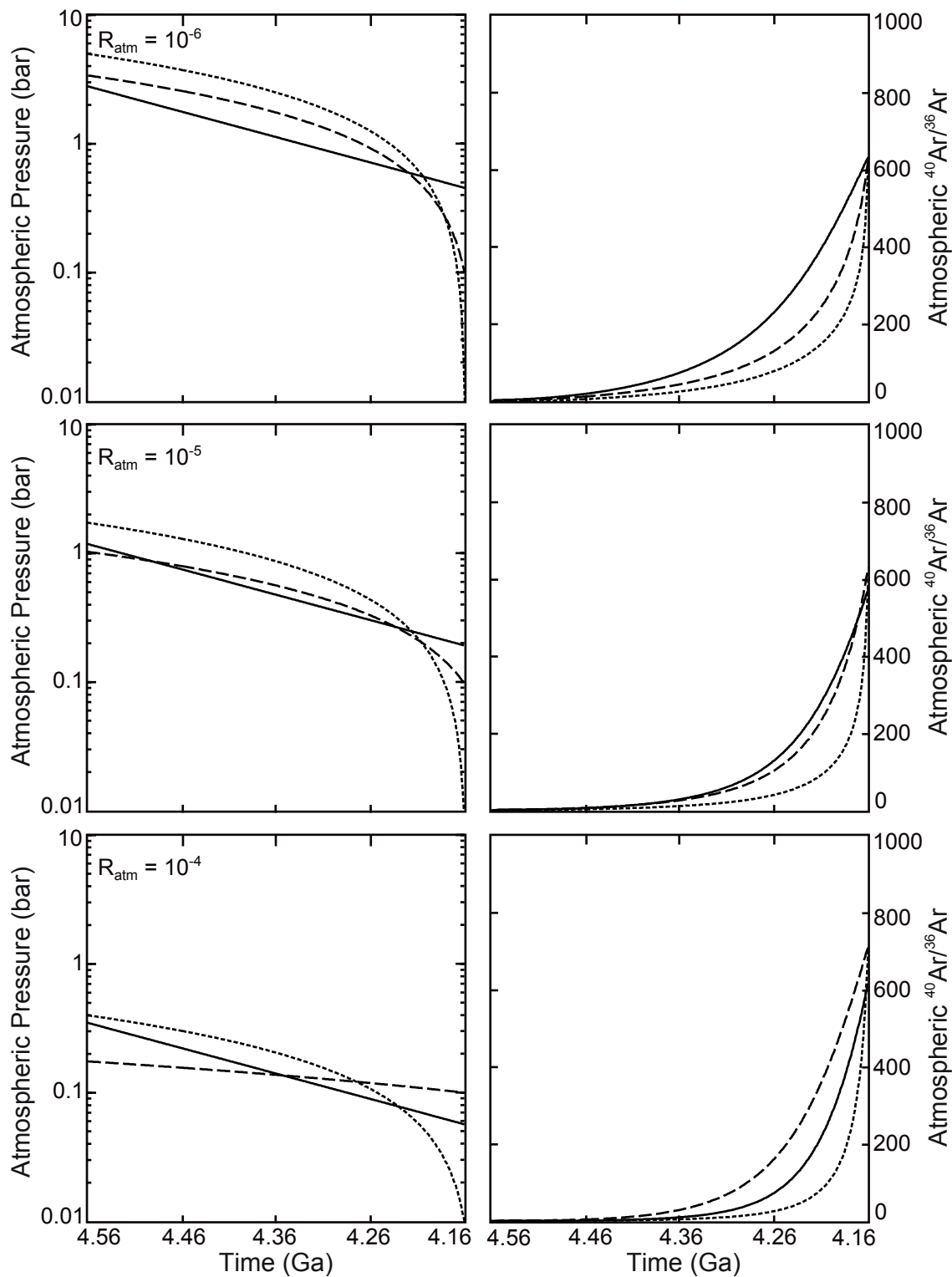


Figure S5: Illustration of the model sensitivity to the primordial concentration of atmospheric ^{36}Ar . Magmas more efficiently elevate the atmospheric $^{40}\text{Ar}/^{36}\text{Ar}$ ratio when the primordial concentration of atmospheric ^{36}Ar is lower. Thus higher atmospheric pressures are required to maintain a given $^{40}\text{Ar}/^{36}\text{Ar}$ ratio if the primordial concentration of atmospheric ^{36}Ar is lowered, and vice versa. The center panels represents our preferred model (modified from Fig. 2 in the main text), wherein the primordial concentration of atmospheric ^{36}Ar is 10 ppb.

Table S1: Summary of trapped $^{40}\text{Ar}/^{36}\text{Ar}$ ratios

Sample	Phase	$^{40}\text{Ar}/^{36}\text{Ar}_i \pm 1\sigma$
ALH 84001 (4.16 ± 0.04 Ga)		
ALH 84001-1	Maskelynite	626 \pm 100
ALH 84001-3	Maskelynite	694 \pm 230
ALH 84001-4	Maskelynite	514 \pm 450
ALH 84001-3	OPX	6 \pm 13
Nakhla (1.33 ± 0.02 Ga)		
Nakhla-1	Plagioclase	676 \pm 4900
Nakhla-2	Plagioclase	2119 \pm 670
Nakhla-5	Plagioclase	2430 \pm 570
Nakhla-1	CPX	42 \pm 10
Nakhla-2	CPX	58 \pm 30
Nakhla-4	CPX	-4 \pm 17
MIL 03346 (1.34 ± 0.01 Ga)		
MIL 03346-1	Mesostasis Glass	1425 \pm 230
MIL 03346-1	CPX	28 \pm 8

Data from Cassata et al. (2010)